Optical spectroscopy and magnetic studies of dimeric europium capronate with 1,10-phenanthroline

Janina Legendziewicz,*[a] Vera Tsaryuk,[b] Vladislav Zolin,[b] Elena Lebedeva,[c] Małgorzata Borzechowska[a] and Mirosław Karbowiak[a]

[a] *Faculty of Chemistry, University of Wrocław, 14 F. Joliot-Curie Str., 50-383, Wrocław, Poland. E-mail: jl@wchuwr.chem.uni.wroc.pl*
[b] *Institute of Radioengineering and Electronics of RAS, Fryazino Moscow reg., 141120, Russia*
[c] *Academy of Fine Chemical Technology, Moscow, Russia*

Received (in Montpellier, France) 13th February 2001, Accepted 5th April 2001
First published as an Advance Article on the web 28th June 2001

Luminescence, excitation of luminescence and absorption spectra of europium capronate crystals as well as vibrational IR and Raman spectra at 4.2, 77 and 293 K were obtained. Magnetic susceptibility measurements were carried out down to 1.7 K. Correlations between the spectral and magnetic properties and details of the structure of the title compound were studied. The crystal field parameters were calculated using the Stark splitting of the Eu^{3+} electronic levels. The oscillator strengths were evaluated. Changes in the spectra and magnetic susceptibility of $Eu(C_5H_{11}COO)_3Phen$ with increasing temperature from 4.2 to 293 K proves transformation of the crystal lattice. The subtle splitting of bands in the regions of the $^5D_0 \rightarrow {}^7F_1$ and $^5D_0 \rightarrow {}^7F_2$ transitions was revealed. Several possible causes of this phenomenon, including resonant vibronic interactions and/or the possible effect of ion-pair interactions, are discussed.

1 Introduction

In the last two decades polynuclear lanthanide compounds have attracted considerable interest.[1–11] This has been motivated by their optical and magnetic properties and their possible applications. Mixed lanthanide carboxylates can be used in the synthesis of nanosize systems and electroluminescent diodes. On the other hand, it is well known that heterocyclic ligands are sensitizers of lanthanide luminescence and mixed LnL_3ph systems (L = charged ligand, ph = heterocyclic diimine) can be used in devices for quantum electronics.[12–14] The important characteristics of these materials result from their bonding character, the donor–acceptor properties of both types of ligands, their structure, the effectiveness of energy transfer and quantum yield of luminescence, as well as ion–ion interactions. Moreover, they are the subject of theoretical investigations of the strengths of electron–phonon coupling and metal–metal interactions.[15–17] Recently, we reported the results of optical and magnetic investigations for a series of polynuclear and heteronuclear systems.[5–9] Now, we present the results of optical and magnetic studies of the dimeric system $Eu(C_5H_{11}COO)_3Phen$ (Phen = 1,10-phenanthroline) to characterise its properties. Calculation of the crystal field (CF) parameters was also performed.

2 Experimental

The Eu(III) mixed compound of formula $[Eu(C_5H_{11}COO)_3(C_{12}H_8N_2)]$ was synthesised according to the procedure described previously.[10] The high-resolution absorption, emission and emission excitation spectra in the 250–720 nm region were recorded at 4.2, 77 and 293 K using a Cary-Varian 5 spectrophotometer equipped with an Oxford 1024 continuous helium cryostat and a SPECTRA-PRO 0.7 m monochromator. The excitation vibronic spectrum in the region of the $^7F_0$-$^5D_0$ transition of Eu^{3+} was obtained with a Rhodamine 6G tuneable dye laser and an MDR-23 monochromator. The intensities of the f–f transition were determined and applied in Judd–Ofelt[18,19] parameter calculations. The energies of CF levels obtained from absorption single crystal spectra and emission spectra were used in CF calculations. Magnetic susceptibility measurements were carried out with a SQUID MPMS5 magnetometer down to 1.7 K. The magnetic susceptibility measurements were corrected for the diamagnetic contributions of the ligands. IR spectra were recorded using a Brucker FS88 FTIR spectrometer (with a resolution of 0.1 cm^{-1}). Raman spectra were recorded on a Nicolet Raman accessory attached to a Nicolet Magna 860 spectrometer. IR and Raman spectra were applied to assign the vibronic lines in the electronic spectra.

3 Results and discussion

Single crystal X-ray diffraction of the title compound confirms its isomorphism with the structure described earlier.[10] The compound crystallizes in a monoclinic system with space group $P2_1/n$ ($Z = 4$) and the following unit cell constants $a = 15.975(2)$, $b = 12.714(2)$, $c = 16.539(2)$ Å, $\beta = 110.76(1)°$.[10] The $Eu(C_5H_{11}COO)_3Phen$ structure consists of binuclear centrosymmetric dimers in which two metal ions are linked by four carboxyl groups, two chelating bridging tridentate and two bridging bidentate. Additionally, two chelating carboxyl groups are coordinated to the metal ions and two M–N(Phen) bonds per metal take the coordination of Eu(III) to nine. Fig. 1 presents a view of lanthanide ion coordination in the crystal.[10] The distorted coordination polyhedron is close to the monocapped square antiprism. A relatively strong deviation of the respective C–C bonds of the capronate radical points to some disorder in the structure which manifests itself in the temperature factors and can lead to a transformation of the structure with decreasing temperature.[10]

IR and Raman spectra of the capronate are presented in Fig. 2. The intense lines in the Raman spectrum are attributed

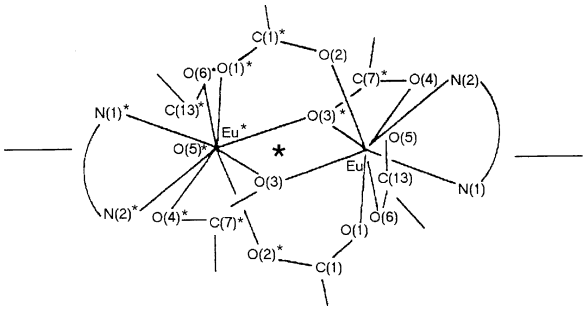

Fig. 1 A view of the lanthanide ion coordination in crystalline $Eu(C_5H_{11}COO)_3Phen$.

to vibrations of the phenanthroline molecules by analogy to complexes of europium nitrates with 1,10-phenanthroline.[20] The different kinds of carboxyl groups existing in the structure can be seen from the IR spectrum. The IR bands at *ca.* 1555 and 1588 cm^{-1} are related to $\nu_{as}(COO^-)$, those at 1430–1460 cm^{-1} to $\nu_s(COO^-)$ stretching vibrations and the bands at 650–670 cm^{-1} to $\delta(COO^-)$ bending vibrations of the capronate groups. Overlapping of bands due to the capronate anion and phenanthroline molecule in the 1400–1460 cm^{-1} region prevents the definitive assignment of the vibrations. The character of COO^- bands in carboxylates is dependent on the carboxylic anion coordination functions and on the degree of inequivalence. The splitting of the $\nu_{as}(COO^-)$, $\nu_s(COO^-)$ and $\delta(COO^-)$ bands demonstrates the inequivalence of the carboxyl groups. Three lines in the $\delta(COO^-)$ region shows the presence of three kinds of carboxyl groups, in agreement with the X-ray data.

The emission excitation spectra of the capronate are shown in Fig. 3. The high-resolution vibronic sideband of the $^7F_0 \rightarrow {}^5D_0$ electronic transition as well as the low-resolution vibronic sideband of the $^7F_0 \rightarrow {}^5D_2$ electronic transitions are presented here. The intense vibronic satellites at *ca.* 435 nm are formed predominantly by the carboxyl group stretching vibrations. A 21.6% population of the $^7F_1$ level at 293 K was determined, explaining the magnetic susceptibility results well (details of which will be discussed below).

The absorption and emission spectra of the capronate at 4.2, 77 and 300 K are shown in Fig. 4 and 5. The relative intensities and splitting of the electronic transitions in these spectra confirm the low point symmetry of the metal centre in the structure. The site symmetry of the metal ions is not higher than C_{2v}. A change in the Stark splitting on increasing the temperature from 4.2 to 300 K is observed, both in the luminescence and absorption spectra. This can be ascribed to the disordering of the positions of atoms in the long aliphatic radical, finally leading to a slight deformation of structure, as was noted in the X-ray investigation.

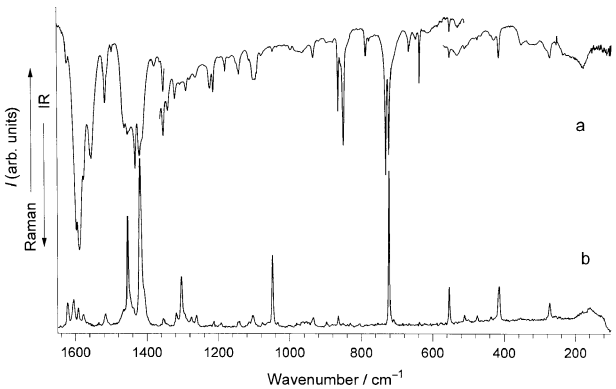

Fig. 2 IR (a) and Raman (b) spectra of $Eu(C_5H_{11}COO)_3Phen$ at 300 K.

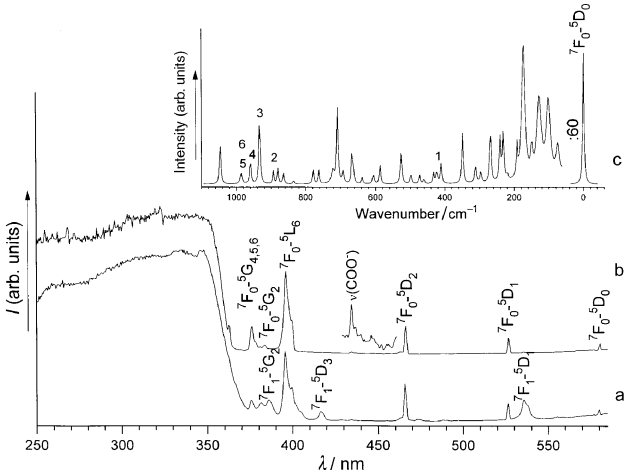

Fig. 3 Excitation spectra of $Eu(C_5H_{11}COO)_3Phen$ at 293 (a) and 77 K (b) and vibronic sideband of the $^7F_0 \rightarrow {}^5D_0$ transition at 77 K (c).

Both C_{2v} and C_s symmetries were applied in the CF calculation. The data-fitting procedures used here are essentially identical to those used previously in energy level analyses of Eu^{3+} in $LaCl_3$ and LaF_3.[21–24] In the calculation, the Reid CF program was applied. The energy parameters included in our calculation are listed in the left-hand column of Table 1 and in footnote a, where ς_{SO} is the radial spin–orbital coupling parameter and $F^k(k = 2, 4, 6)$ are Slater electrostatic parameters. The α, β, γ, T^i $(i = 2–8)$, M^k $(k = 0, 2, 4)$ and P^k $(k = 2, 4, 6)$ parameters were defined according to the convention used in ref. 21, 22 and 24. In all our calculations, we assumed the following relationships for M^k: $M^2 = 0.56M^0$, $M^4 = 0.38M^0$, along with $P^4 = 0.5P^2$ and $P^6 = 0.1P^2$. The empirical databases available for the analysed system were not

Table 1 Free ion and crystal field parameters

Parameter[a]	C_s [b,c]/cm^{-1}	C_{2v} [b,d]/cm^{-1}
E_{avg}	63 815(23)	63 798(20)
F^2	82 900(32)	82 900(28)
F^4	59 189(71)	58 531(60)
F^6	42 885(55)	43 338(47)
ζ	1337(5)	1339(4)
B_0^2	−276(26)	−326(24)/−277
B_2^2	−119(21)	94(17)/84
B_0^4	235(32)	−585(32)/−715
B_2^4	[28][e]	346(20)/179
$Im\ B_2^4$	−189(31)	
B_4^4	295(39)	101(22)/253
$Im\ B_4^4$	200(57)	
B_0^6	201(42)	590(32)/647
B_2^6	[30][e]	919(27)/650
$Im\ B_2^6$	−127(41)	
B_4^6	101(84)	−451(24)/−186
$Im\ B_4^6$	730(43)	
B_6^6	−259(75)	151(25)/353
$Im\ B_6^6$	−406(73)	
n	49	49
σ[e]	14.0	12.1

[a] Values of the free ion parameters, which were kept constant during fitting procedure: $\alpha = 20.16$, $\beta = -567$, $\gamma = 1500$; $T^2 = 300$, $T^3 = 40$, $T^4 = 60$, $T^6 = -300$, $T^7 = 370$, $T^8 = 320$; $M^0 = 2.1$, $M^2 = 1.18$, $M^4 = 0.65$; $P^2 = 360$, $P^4 = 180$, $P^6 = 36.0$. [b] Values in parentheses are the errors in each parameter. [c] Values of the B_2^4 and B_2^6 parameters were kept at constant B_2^4/B_0^4 and B_2^6/B_0^6 ratios of 0.12 and 0.15, respectively, during the fitting procedure for C_s symmetry as a result of geometrical considerations. [d] Numbers after a solidus indicate values calculated for the C_{2v} site symmetry without inclusion of J–J mixing. [e] Deviation: $\sigma = \Sigma[\Delta_i^2/(n-p)]^{1/2}$, where Δ_i is the difference between the observed and calculated energies, n is the number of levels fitted and p is the number of parameters freely varied.

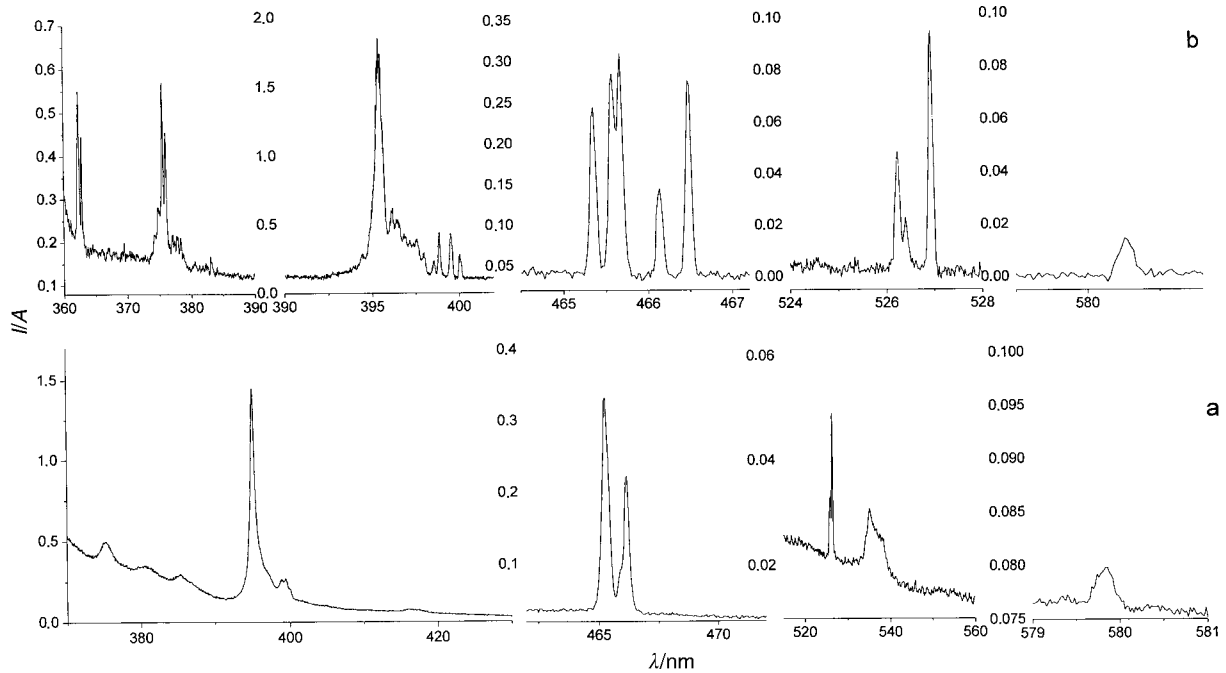

Fig. 4 Absorption spectra of $Eu(C_5H_{11}COO)_3Phen$ at 293 (a) and 4 K (b).

extensive enough to support analyses in which all the energy parameters listed in Table 1 could be treated as 'freely varying fitting parameters'. Inclusion of all of the B_q^k parameters into the fitting procedure resulted in low and poorly determined values for the C_2^4 and C_2^6 parameters, thus in final step of calculations those two parameters were constrained by C_2^4/C_0^4 and C_2^6/C_0^6 ratios, equal to 0.12 and 0.15, respectively, found from geometrical considerations. The crystal field parameters obtained in the C_{2v} fitting were the starting point for the C_s refinement. The crystal field Hamiltonian for C_s point symmetry contains 14 B_q^k parameters. The $Im\ B_2^2$ was set to zero by an appropriate choice of coordinate system.

The values assigned to the fixed parameters were taken from the analysis of the LaF_3 : Eu system by Carnall *et al.*[25] The numbers of empirical energy levels used in our parameter-fit calculations are given in the second column of Table 2. The parameter values used in our final energy level calculation are listed in Table 1 for C_{2v} symmetry and C_s symmetry. In addition, the values of CF parameters calculated without including *J*-mixing are presented in this table. The deviations of our final calculated energy levels from the experimental ones are listed in the columns of Table 2. Note the relatively low Δ

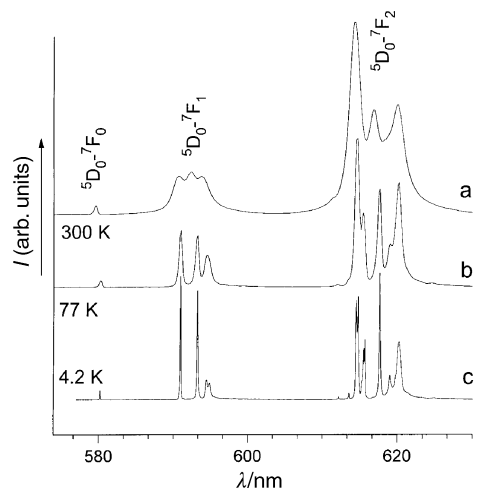

Fig. 5 Luminescence spectra of $Eu(C_5H_{11}COO)_3Phen$ at 300 (a), 77 K (b) and 4 K (c).

deviation of the energy levels for europium, where we used 49 (of 60) Stark components in our calculations; spanning 11 spin–orbit coupling levels in absorption and emission spectra at 4.2 K, these multiplets were derived primarily from four Russel–Saunders terms (^7F, ^5D, ^5L and ^5G). Note also the significant differences between the two sets of CF parameters calculated for C_{2v} and C_s symmetries due to the differences in the corresponding models. The differences between these values and those calculated excluding *J*-mixing can be attributed to limitations of the simple point charge electrostatic model. At the same time, it is important to notice the radical variation (change of sign) of the axial B_0^2 parameter of the second order, calculated using the same routine, at transition to mixed $Ln\beta_3Phen$ systems (β = β-diketone) previously reported by us.[13,14] This variation reflects the changes in the coordination polyhedra of the lanthanide ions. At the same time the CF parameters of the sixth order change more regularly, suggesting that the immediate environments of the metal ions in these compounds are related.

Analysis of the emission spectra recorded at 4.2 K (Fig. 5) is similarly illustrative. Subtle splitting of bands in the range of the $^5D_0 \rightarrow {}^7F_1$ and $^5D_0 \rightarrow {}^7F_2$ transitions is observed. This splitting could be the result of structural transformation, as mentioned in the discussion of X-ray data, but also due to the resonant vibronic effect. In adddition, the above phenomena could also be overlapped with the cooperative M–M interaction in the dimeric system. Considering the values of the splitting (4–10 cm^{-1}), deformation of the dimers and non-equivalency of two Eu(III) ions created in this way, is a reasonable interpretation. This transformation will be the subject of further investigation in the 293–4.2 K temperature range. Cooperative effects for a system with a large M–M distance seem to be less important. Resonance effects, with participation of the ν(C–C) (937, 962 cm^{-1}) vibrations and $\sigma(COO^-)$ modes of the capronate anion, as well as phenanthroline modes, associated with the $^5D_0$–$^7F_0$ transition, (lines 1–7 in Fig. 6), are more probable. The frequencies of these vibrations are in agreement with the positions of vibronic satellites 1–6 in the anti-Stokes sideband of the $^7F_0$–$^5D_0$ transition (Fig. 3). Thus, we have a case of resonance under conditions of low (lines 2, 3, 5 and 7 in Fig. 6) and strong (lines 1, 4 and 6) nonadiabaticity simultaneously. The vibronic lines 1, 4, 6 borrow around 50% of the intensity of the neighbouring zero-

Table 2 Calculated and experimental energy levels

SLJ State[a]	Experimental energy/cm^{-1}	$E_{exp.} - E_{calc.}$[b] for C_s/cm^{-1}	$E_{exp.} - E_{calc.}$[b] for C_{2v}/cm^{-1}
$^7F_0$	0	7	−7
$^7F_1$	312	−6	−6
	378	5	−6
	412	−21	−3
$^7F_2$	966	−15	−11
	992	−15	−11
	1045	13	31
	1080	18	18
	1111	−4	−17
$^7F_3$	1848	0	3
		1854	1865
		1876	1867
		1889	1877
	1905	1	−7
		1931	1928
		1946	1946
$^7F_4$	2715	−1	2
	2778	15	9
	2818	10	−4
		2861	2823
		2886	2895
	2903	12	3
		2919	2909
	2932	0	2940
	3070	−6	0
$^7F_5$		3800	3794
		3820	3797
		3856	3839
		3904	3865
		3906	3920
		3923	3957
		3959	3970
		3997	3987
		4028	4012
		4040	4058
		4087	4059
$^7F_6$		4903	4910
		4911	4924
		4943	4941
		4967	4964
		4992	4992
		5021	4993
		5049	5010
		5068	5050
		5069	5051
		5091	5102
		5103	5113
		5116	5128
		5120	5134
$^5D_0$	17 234	−2	−9
$^5D_1$	18 977	6	5
	18 997	9	3
	19 003	−1	1
$^5D_2$	21 437	−18	−12
	21 453	−2	0
	21 474	9	5
	21 479	10	9
	21 489	8	12
$^5D_3$		24 330	24 332
		24 340	24 338
		24 352	24 351
		24 361	24 354
		24 362	24 358
		24 372	24 360
		24 373	24 379
$^5L_6$	24 997	−25	−15
	25 030	3	−7
			25 049
	25 071	−6	−8
	25 090	10	5
		25 122	
	25 127	5	22
	25 152	3	1
		25 153	
	25 178	−1	9
	25 198	3	−4
	25 222	1	−10
	25 241	12	−7
			25 266
	25 290	−37	1
$^5L_7{}^+$		26 047	26 047
$^5G_2{}^+$		26 077	26 067

Table 2 Continued

SLJ State[a]	Experimental energy/cm^{-1}	$E_{exp.} - E_{calc.}$[b] for C_s/cm^{-1}	$E_{exp.} - E_{calc.}$[b] for C_{2v}/cm^{-1}
$^5G_3{}^+$		26 108	26 084
$^5G_4{}^+$	26 110	0	6
$^5G_5{}^+$		26 120	26 116
$^5G_6$		26 136	26 117
		26 141	26 119
		26 149	26 156
		26 165	26 202
		26 191	26 212
		26 201	26 218
		26 221	26 220
		26 225	26 225
		26 259	26 258
	26 277	11	6
		26 327	26 360
		26 365	26 367
		26 391	26 391
		26 406	26 394
	26 433	2	5
		26 452	26 447
	26 462	0	4
		26 469	26 470
		26 475	26 491
		26 484	26 500
	26 520	5	10
		26 553	26 551
		26 574	26 587
		26 581	2591
	26 594	11	0
		26 599	26 597
		26 601	26 602
		26 607	26 603
		26 612	26 604
		26 626	26 618
			26 619
	26 627	0	−2
		26 639	26 634
		26 645	26 644
		26 647	26 647
		26 658	26 651
		26 659	26 661
		26 669	26 670
	26 677	7	6
		26 678	26 676
		26 682	26 679
		26 688	26 695
		26 693	26 701
		26 696	26 702
		26 708	26 712
		26 710	26 714
		26 711	26 717
		26 717	
	26 724	−2	−3
		26 728	26 732
		26 730	26 737
		26 736	26 749
		26 740	26 753
		26 755	26 758
		26 765	26 773
		26 767	26 776
		27 062	27 057
		27 065	27 064
		27 095	27 065
		27 102	27 077
		27 106	27 086
		27 107	27 105
		27 144	27 145
		27 153	27 151
		27 157	27 162
		27 169	27 163
		27 183	27 193
		27 185	27 194
		27 190	27 201
		27 195	27 210
		27 205	27 211
		27 214	27 217
		27 216	27 224
$^5D_4$	27 562	−19	−25
	27 601	8	−1
	27 615	−7	12

[a] The leading eigenvector component is shown. [b] Where any experimental level can be assigned, the calculated energy value is indicated instead of Δ.

phonon lines. Careful analysis of the absorption spectra at 4.2 K could exclude the latter effect, but the intensities of the absorption lines are especially low, making detection of subtle splitting impossible. Highly effective energy transfer processes strengthen the intensities of the emission lines, which are, as a result, excellently resolved. Thus, several phenomena can affect the emission spectra of the system under investigation.

Table 2 gives values for the splitting of the levels, so that the $^7F_1$ and $^7F_2$ levels are separated from $^7F_0$ by 312 and by 966 cm^{-1}, respectively. These two levels can be partially populated at 293 K, which manifests itself in the absorption as well as in the emission excitation spectra (Fig. 3 and 4).

Considering the $^5D_0 \rightarrow {}^7F_J/{}^5D_0 \rightarrow {}^7F_0$ emission intensity ratio, the absolute values of transition oscillator strengths from the $^7F_0 \rightarrow {}^5D_0$ transition determined from the absorption can be evaluated. Thus, a large set of the transition intensities can be used in Judd–Ofelt parameter calculations including those of the $^7F_1 \rightarrow {}^5D_4$ and $^7F_0 \rightarrow {}^5D_4$ transitions (recalculated from the 4.2 K absorption measurements—Table 3). Table 3 collects the oscillator strength values used in the calculations and the τ_λ (Ω_λ) parameters determined with an excellent accuracy, as for Eu(III). Comparison of the results of the intensity analysis with data previously reported[8] for crystalline $Eu(CCl_3COO)_3 \cdot 2H_2O$ highlights the higher intensities of all the f–f transitions in the present system. Reducing the temperature leads to an increase in the intensities of some lines, which is in agreement with depopulation of the $^7F_1$ and $^7F_2$ levels, but for some lines, their intensities decrease ($^7F_0 \rightarrow {}^5D_2$). This irregularity indicates an anisotropy of the polarizability of the Phen molecules contribution and, as a result, the strongest effect is observed for levels with $\Delta J = 2$, the most affected by the polarizability. Additionally, according to the vibronic transition probability,[14,26] the strongest electron–phonon coupling should be observed for this transition as well. Thus, reducing the temperature can lead to a larger decrease in the intensity of this transition. These opposite effects are manifested as irrregularities in the changes in intensity (see Table 3).

The magnetic data of the dimeric system are also worth analysing. In the free-ion approximation, the molar magnetic susceptibility for a mononuclear species is given by the relation described in ref. 27 and 28. For rare earth systems, the $\chi_M T$ *vs.* T plot deviates from the relation predicted by theory[27,28] due to the crystal field effect, which can remove the $2J + 1$ degeneracy of the ground state, and by thermal population of free-ion excited states, this last effect can appear in our Eu(III) system. The high-temperature limit $(\chi_M T)_{HT}$, for $kT \gg \lambda$, can be obtained by assumption following the work of Kahn,[29] that the susceptibility of the ^7F term is a sum of the orbital contribution and the spin contribution and can be equal to $12N\beta^2/k$, *i.e.* 4.5 cm^3 K mol^{-1}. This limit has never been reached, for either isolated, polynuclear or Cu : Ln heteronuclear systems because only the first two terms of Eu(III) ($^7F_1$ and $^7F_2 \approx 1\%$) can be significantly populated and, in our case, where the energies of the $^7F_1$ and $^7F_2$ terms are located at 312 and 966 cm^{-1}, we obtained a result of 1.2 cm^3 mol^{-1} K. At the low temperature limit, $\chi_M T$ should be zero because the $^7F_0$ ground state is nonmagnetic, but it is finite as a result of coupling between the $^7F_0$ and $^7F_1$ states through Zeeman perturbation. The χ_M *vs.* T and $\chi_M T$ *vs.* T plots for europium capronate are shown in Fig. 7. The values of χ_M in the range 120–40 K remain unchanged and equal to 5.4×10^{-3} cm^3 mol^{-1} and are higher than for polynuclear polymeric $Eu(CCl_3COO)_3 \cdot 2H_2O$.[8] $\chi_M T$ is 1.25 cm^3 mol^{-1} K, also a little higher, which indicates the difference in splitting of the levels in both the systems considered. At the low temperature limit, according to the Caro and Porcher relation,[30] $(\chi_M)_{LT}$ can be calculated using λ determined from spectroscopic measurements. At the low temperature limit using Caro and Porcher's simple relation $(\chi_M)_{LT} = 2.086 \times 10^3/\lambda$ and since below 75 K

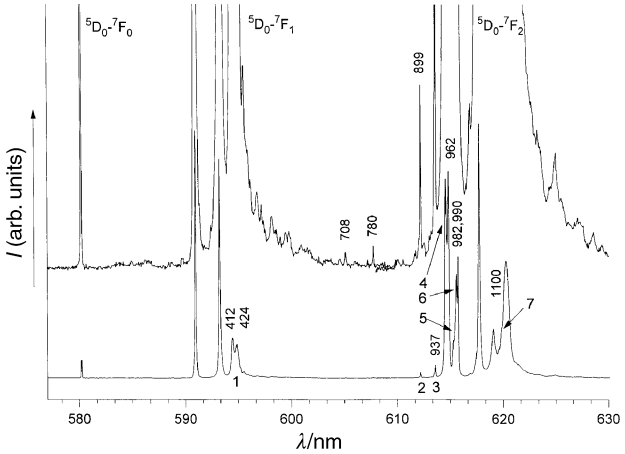

Fig. 6 The resonance effect in the $^5D_0 \rightarrow {}^7F_1$ and $^5D_0 \rightarrow {}^7F_2$ transitions in the emission spectra of $Eu(C_5H_{11}COO)_3Phen$ at 4.2 K.

Table 3 The experimental oscillator strength values ($P \times 10^8$) for the f–f transitions, $\tau_\lambda \times 10^9$ and $\Omega_\lambda \times 10^{20}$ for crystalline $Eu(C_5H_{11}COO)_3Phen$. $\tau_2 \times 10^9 = 2.90 \pm 1.96$; $\tau_4 \times 10^9 = 5.07 \pm 2.64$; $\tau_6 \times 10^9 = 4.07 \pm 0.24$. $\Omega_2 \times 10^{20} = 2.05 \pm 1.39$; $\Omega_4 \times 10^{20} = 3.59 \pm 1.87$; $\Omega_6 \times 10^{20} = 2.88 \pm 0.17$

		$P \times 10^8$	
Transition	Spectral region/nm	298 K	4.2 K
$^7F_1 \rightarrow {}^5D_0$	590–592	0.21	—
$^7F_0 \rightarrow {}^5D_0$	579–581	0.06	0.24
$^7F_1 \rightarrow {}^5D_1$	530–548	4.70	—
$^7F_0 \rightarrow {}^5D_1$	525–528	1.64	2.31
$^7F_0 \rightarrow {}^5D_2$	463–468	15.011	13.32
$^7F_1 \rightarrow {}^5D_3$	412–430	6.79	—
$^7F_1 \rightarrow {}^5L_6$	398–405	37.05	—
$^7F_0 \rightarrow {}^5L_6$	391–398	210.05	356.81
$^7F_1 \rightarrow {}^5G_2$	384–391	28.64	—
$^7F_0 \rightarrow {}^5G_2$	378–384	23.13	—
$^7F_0 \rightarrow {}^5G_{(4,5,6)}$	373–378	33.17	87.31
$^7F_1 \rightarrow {}^5D_4$	378–364	6.28[a]	—
$^7F_0 \rightarrow {}^5D_4$	361–364	28.74[a]	39.87
$^7F_1 \leftarrow {}^5D_0$		2.52	—
$^7F_2 \leftarrow {}^5D_0$		7.28	—
$^7F_3 \leftarrow {}^5D_0$		0.09	—
$^7F_4 \leftarrow {}^5D_0$		1.29	—

[a] Oscillator strength values recalculated from 4.2 K absorption measurements.

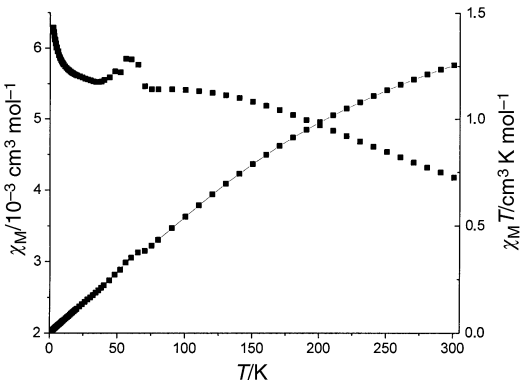

Fig. 7 Experimental magnetic data plotted as χ_M *vs.* T (■) and $\chi_M T$ *vs.* T (-■-), calculated per molecule of $Eu(C_5H_{11}COO)_3Phen$.

$\chi_M T$ varies linearly with T, from the slope χ_M can be calculated as 6×10^{-3} cm^3 mol^{-1}. From the above equation, λ can be estimated, which gives a value of 347 cm^{-1}. The energy gap between $^7F_0$ and $^7F_1$ was found to be 367 cm^{-1}, thus proving that this approximation is quite good.

Let us compare the magnetic values obtained here with earlier data determined for $Eu(CCl_3COO)_3 \cdot 2H_2O$ with a similar dimeric unit but a polymeric structure.[8]

Our values of χ_M are higher and show some irregularities at 70–40 K. This suggests a structural transformation, confirming the conclusions arising from the spectroscopic investigation and X-ray data. This effect is also overlapped by deviation of the measurement due to air sealed in the tube. Moreover, the larger value of χ_M for the title dimer system could reflect the absence of the supplementary effect of the polymeric structure, which is created by coupling of the dimeric units by further carboxylic bridges in an endless chain in europium trichloroacetate. Furthermore, both the dimeric and polynuclear systems exhibit lower values of χ_M in the respective T regions in comparison to the monomeric Eu(III) monomeric system reported by Kahn.[29] In the low temperature range (0–75 K), the magnetic moment is relatively low, the electrons of coupled ions can interact, as a result a decrease in the $\chi_M T$ and χ_M values is observed. At very low temperatures (below 8 K), a dramatic increase in χ_M is observed, most probably caused by a small amount of paramagnetic impurities.

Conclusion

Analysis of the electronic transition probabilities and CF parameters indicate similarities between $Ln(C_5H_{11}COO)_3Phen$ and the $Ln\beta_3Ph$ systems investigated earlier. Good agreement was found between the $^7F_0$–$^7F_1$ splittings determined on the basis of magnetic and spectroscopic studies.

Magnetic and spectroscopic results for the investigated dimeric system show a structural transformation at *ca.* 40–70 K. Subtle splitting of bands in the regions of the $^5D_0 \rightarrow {}^7F_1$ and $^5D_0 \rightarrow {}^7F_2$ transitions was found. The resonant vibronic interaction and/or weak effect of interacting metal ions could be among the various causes of this splitting. Comparison of spectroscopic and magnetic results with those obtained previously for a polymeric Eu(III) compound and a monomeric system was made.

Acknowledgements

The work was supported by the Polish State Committee for Scientific Research (KBN) and by the Russian Foundation for Basic Research (grant N 00-02-16655).

References

1 J. Legendziewicz, *Acta Phys. Pol. A*, 1996, **90**, 127.
2 V. I. Tsaryuk, V. F. Zolin and L. G. Koreneva, *Koord. Khim.*, 1977, **3**, 183.
3 A. Panagiotopoulus, T. F. Zafiropoulus, S. P. Perlepes, B. Bakalbasis, J. Masson-Ramade, O. Kahn, A. Terzis and C. P. Raptopoulu, *Inorg. Chem.*, 1995, **34**, 4918.
4 C. Benelli, A. Caneschi, D. Gatteschi and L. Pradi, *Mater. Chem. Phys.*, 1992, **31**, 17.
5 G. Oczko, J. Legendziewicz, J. Mroziński and G. Meyer, *J. Alloys Compd.*, 1998, **275**, 219.
6 J. Legendziewicz, M. Borzechowska, G. Oczko and J. Mroziński, *Spectrochim. Acta, Part A*, 1998, **54**, 2197.
7 J. Legendziewicz, M. Borzechowska, G. Oczko and G. Meyer, *New J. Chem.*, 2000, **24**, 53.
8 J. Legendziewicz and M. Borzechowska, *J. Alloys Compd.*, 2000, **300–301**, 353.
9 Yu. Yablokov, V. K. Voronkova, J. Legendziewicz, E. Huskowska, G. Oczko and M. Borzechowska, *Appl. Magn. Reson.*, 2000, **18**, 165.
10 M. A. Porai-Koshits, A. S. Antsyshkina, G. G. Sadikov, E. N. Lebedeva, S. S. Korovin, R. N. Shchlelokov and V. G. Lebedev, *Zh. Neorg. Khim.*, 1995, **40**, 748.
11 S. S. Korovin, E. N. Lebedeva, O. Yu. Tkachenko and M. G. Zaytseva, *Zh. Neorg. Khim.*, 1999, **44**, 753.
12 V. Tsaryuk, V. Zolin and J. Legendziewicz, *Spectrochim. Acta, Part A*, 1998, **54**, 2247.
13 V. Tsaryuk, J. Legendziewicz, V. Zolin, L. Puntus and J. Sokolnicki, *9th Cimtec World Forum on New Materials*, ed. P. Vincenzini and G. C. Righini, Symp. 10, Techna Srl., 1999, p. 299–306.
14 J. Legendziewicz, *J. Alloys Compd.*, 2000, **300–301**, 71.
15 O. L. Malta, *J. Phys. Chem.*, 1995, **56**, 1053.
16 M. Błażej and W. Stręk, in *Excited States of Transition Elements*, ed. W. Stręk, W. Ryba-Romanowskí, J. Legendziewicz and B. Jeżowska-Trzebiatowska, World Scientific Publishing Co. Pte. Ltd., Singapore, 1992, p. 308.
17 B. Jeżowska-Trzebiatowska, J. Legendziewicz and W. Stręk, *Inorg. Chim. Acta*, 1984, **95**, 157.
18 B. R. Judd, *Phys. Rev.*, 1962, **127**, 750.
19 G. S. Ofelt, *J. Chem. Phys.*, 1962, **37**, 511.
20 V. Tsaryuk, V. Zolin, L. Puntus, V. Savchenko, J. Legendziewicz, J. Sokolnicki and R. Szostak, *J. Alloys Compd.*, 2000, **300–301**, 184.
21 H. M. Crosswhite, H. Crosswhite, F. W. Kaseta and R. Sarup, *J. Chem. Phys.*, 1976, **64**, 1981; W. T. Carnall, H. Crosswhite, H. M. Crosswhite and J. G. Conway, *J. Chem. Phys.*, 1976, **64**, 3582.
22 W. T. Carnall, J. V. Beitz, H. Crosswhite, R. Rajnak and J. B. Mann, *Systematics and the Properties of Lanthanides*, ed. S. P. Sinha, Redel, Boston, 1983, p. 389–450.
23 H. M. Crosswhite, in *Spectroscopie des Elements de Transition et des Elements*, Lourds dans les Solides, CNRS, Paris, 1977, p. 65.
24 W. T. Carnall, H. Crosswhite and H. M. Crosswhite, *Argonne Nat. Lab., Tech. Rep.*, 1977.
25 W. T. Carnall, G. L. Goodman, K. Rajnak and R. S. Rana, *Argonne Nat. Lab., Tech. Rep.*, 1988.
26 G. Blasse, *Int. Rev. Phys. Chem.*, 1992, **11**, 71.
27 A. P. Casey, in *Theory of Applications of Molecular Paramagnetism*, ed. E. A. Bondreaux and L. N. Mulay, John Wiley, New York, 1976, p. 135.
28 O. Kahn, *Molecular Magnetism*, VCH, New York, 1993.
29 M. Andruh, E. Bakalbassis, O. Kahn, J. C. Trombe and P. Porcher, *Inorg. Chem.*, 1993, **32**, 1616.
30 P. Caro and P. Porcher, *J. Magn. Mater.*, 1986, **58**, 61.